Marginal Stability of the Convective Boundary Layer

JOHN THUBURN AND GEORGIOS A. EFSTATHIOU

University of Exeter, Exeter, United Kingdom

(Manuscript received 30 June 2018, in final form 30 April 2019)

ABSTRACT

We hypothesize that the convective atmospheric boundary layer is marginally stable when the damping effects of turbulence are taken into account. If the effects of turbulence are modeled as an eddy viscosity and diffusivity, then an idealized analysis based on the hypothesis predicts a well-known scaling for the magnitude of the eddy viscosity and diffusivity. It also predicts that the marginally stable modes should have vertical and horizontal scales comparable to the boundary layer depth. A more quantitative numerical linear stability analysis is presented for a realistic convective boundary layer potential temperature profile and is found to support the hypothesis.

1. Introduction

Large-eddy simulations (LESs) of the dry convective boundary layer, with homogeneous bottom boundary conditions and in the absence of mean wind, are found to be dominated by plumes and thermals whose horizontal and vertical scales are comparable to the boundary layer depth z_* (e.g., Schmidt and Schumann 1989). These length scales seem to require some explanation, given that when the equations of inviscid fluid dynamics are linearized about a convectively unstable basic state, the largest growth rates are found for the smallest horizontal scales [e.g., Emanuel (1994), chapter 3, in the limit of large Rayleigh number].

Observations of convective boundary layers in the real world also often show structures with horizontal and vertical scales comparable to z_* (e.g., Tennekes and Lumley 1972; Garratt 1992). Structures with much larger horizontal scale (aspect ratios up to 20 or 30) such as rolls and open and closed cells, are also observed, especially in cloudy boundary layers over the ocean (e.g., Atkinson and Zhang 1996) though there remain many open questions related to the roles of shear, moisture, radiation, and inhomogeneous boundary conditions, for example, in determining these structures.

Experiments and simulations of Rayleigh–Bénard convection, the classic prototypical convection problem, at high Rayleigh numbers also show the emergence of ''superstructures'' with horizontal scale around 6–7 times the domain depth (e.g., Pandey et al. 2018; Stevens et al. 2018). Again, there are open questions, for example, regarding the role of a finite Rayleigh number, in our understanding of these superstructures. Also, there are some key difference between Rayleigh–Bénard convection and the convective boundary layer. First, Rayleigh–Bénard convection has symmetrical lower and upper boundary conditions and a mean heat flux that is independent of height, whereas the convective boundary layer is capped by an inversion layer where the heat flux goes to zero. Second, in the convective boundary layer the turbulent length scale adjacent to the lower boundary is assumed to be determined by a roughness length z_0, rather than molecular viscosity and diffusivity, and hence the Rayleigh number does not enter the problem.

In this note we leave aside many of these complexities of real-world convection and of Rayleigh–Bénard convection and focus on the dry convective boundary layer with homogeneous bottom boundary conditions and in the absence of mean wind. Although this idealized case may only be exactly realizable in LES or direct numerical simulation, we believe the ideas put forward may still have some real-world relevance.

Under steady forcing of the convective boundary layer with homogeneous boundary conditions, the time scale for the evolution of the horizontal mean state and the statistics of the turbulence is much longer than the individual eddy turnover time. In other words, a turbulent quasi equilibrium is established. This quasi equilibrium is maintained by a robust negative feedback: stronger turbulence will quickly lead to a stronger turbulent cascade

Corresponding author: John Thuburn, j.thuburn@exeter.ac.uk

DOI: 10.1175/JAS-D-18-0222.1

and dissipation of turbulent kinetic energy, and vice versa for weaker turbulence.

In this quasi equilibrium, eddies of any given scale will extract energy from (or perhaps lose energy to) the stratification of the mean state, and, in general, will both transfer energy to and receive energy from eddies of other scales through nonlinear turbulent interactions. Let us conceptually separate these latter two and refer to them as the turbulent forcing effect and the turbulent damping effect, respectively. At any given scale, the interaction with the mean state and the turbulent forcing and damping effects must balance, to a good approximation.

Now consider the behavior of eddies of some given scale. If we neglect the turbulent forcing effect at that scale, then those eddies must be damped, or at least not grow, as a result of interaction with the mean state and turbulent damping. If the turbulent damping effect could be taken into account in a linear stability analysis, then we must find that, in contrast to the purely inviscid linear case, all modes are either damped or marginally stable.

In this note we discuss the hypothesis that there is a single scale at which such linear modes are marginally stable. The marginal stability hypothesis is interesting for several reasons. With a plausible assumption about the form of the turbulent damping, it leads to the prediction that the horizontal and vertical scale of the marginal modes should be comparable to z_*. It also predicts a well-known scaling for the strength of the damping effect. Moreover, it implies that eddies on the scale of the marginal mode are maintained by a balance between instability of the mean state and turbulent damping, with negligible turbulent forcing from eddies of other scales; thus, it has implications for the direction of spectral energy transfer by turbulence at different scales.

Similar marginal stability ideas have been applied in other contexts. The idea that deep convection acts to quickly restore a moist convectively unstable atmospheric profile to neutrality through much of the troposphere is well known (e.g., Emanuel et al. 1994), and this "convective adjustment" idea is the basis for some parameterizations of convection in weather and climate models (e.g., Betts and Miller 1986; Emanuel 1994). An analogous idea has been proposed for baroclinic instability (Stone 1978; Lindzen and Farrell 1980). However, it is not so straightforward to determine whether the mean atmospheric state is close to baroclinic marginal stability. Moreover, the time scale for the baroclinic adjustment process is comparable to the time scales of the processes, such as radiation, that force the mean state toward instability (Barry et al. 2000). This has motivated some authors to propose that the atmosphere undergoes a "weak baroclinic adjustment" in which a nonlinear turbulent equilibrium is reached even though the mean state is unstable to linear modes (Vallis 1988; Stone and Branscombe 1992). Our hypothesis for the convective boundary layer might be considered a variation on this weak adjustment idea. An attractive feature, though, is that the damping effect of the nonlinear turbulence can be modeled and taken into account in a quantitative linear stability analysis.

In discussing marginal stability it is important to note that we are concerned with perturbations to a state of fully developed turbulence, not to a state of rest. In section 2 we write down the equations governing such perturbations. To make progress, it is proposed that the turbulent damping effect can be modeled by an eddy viscosity and diffusivity.

In section 3 we consider an idealized situation with uniform unstable stratification and uniform eddy viscosity and diffusivity with a turbulent Prandtl number = 1. These assumptions are crude and unrealistic and are made for mathematical convenience in order to confirm the general plausibility of the hypothesis. Nevertheless, similar analyses have proved useful in diagnosing the onset of resolved boundary layer convection in numerical models (Piotrowski et al. 2009; Ching et al. 2014). With these assumptions, the marginal stability hypothesis predicts that the strength of the eddy viscosity should scale like $z_* w_*$, where w_* is a convective velocity scale, in agreement with well-known convective boundary layer scaling theory (e.g., Holtslag 1998). It also predicts that the vertical and horizontal scales of the marginal mode should be comparable to z_*.

In section 4 we perform a direct check on the marginal stability hypothesis by carrying out a numerical linear stability analysis for a realistic convective boundary layer potential temperature profile taken from a large-eddy simulation, and using a typical convective boundary layer eddy viscosity profile. The results are found to be consistent with the marginal stability hypothesis.

2. Linearized equations

Assume that the evolving turbulent state of a convective boundary layer satisfies the nonlinear Boussinesq equations:

$$\frac{\partial \mathbf{u}}{\partial t} + \nabla P - b\hat{\mathbf{z}} = -\mathbf{u}\cdot\nabla\mathbf{u}, \tag{1}$$

$$\frac{\partial b}{\partial t} + wN_0^2 = -\mathbf{u}\cdot\nabla b, \tag{2}$$

$$\nabla\cdot\mathbf{u} = 0. \tag{3}$$

Here $\hat{\mathbf{z}}$ is the vertical unit vector, $\mathbf{u}$ is the velocity vector, P is the modified pressure, $b = g(\theta - \theta_0)/\theta_{00}$ is the buoyancy, and $N_0^2 = (g/\theta_{00})\partial\theta_0/\partial z$ is the background buoyancy frequency squared, where g is the gravitational acceleration, θ_{00} is a constant reference potential temperature, and $\theta_0(z)$ is a background potential temperature profile. A perturbed state given by $\mathbf{u} + \mathbf{u}'$, $P + P'$, and $b + b'$ will obey analogous equations. Subtracting the perturbed equations from the original equations gives the following equations for the evolution of the perturbations:

$$\frac{\partial \mathbf{u}'}{\partial t} + \nabla P' - b'\hat{\mathbf{z}} = -\nabla \cdot (\mathbf{u}\mathbf{u}' + \mathbf{u}'\mathbf{u} + \mathbf{u}'\mathbf{u}'), \tag{4}$$

$$\begin{aligned}\frac{\partial b'}{\partial t} + w'N^2 &= -\mathbf{u}' \cdot \nabla(b - \overline{b}) - \mathbf{u} \cdot \nabla b' - \mathbf{u}' \cdot \nabla b' \\ &= -\nabla \cdot [\mathbf{u}'(b - \overline{b}) + \mathbf{u}b' + \mathbf{u}'b'],\end{aligned} \tag{5}$$

$$\nabla \cdot \mathbf{u}' = 0. \tag{6}$$

Here $\overline{b}$ is the horizontal mean buoyancy. We have added $w'\partial\overline{b}/\partial z$ to both sides of (5) and defined $N^2 = N_0^2 + \partial\overline{b}/\partial z$ so that the left-hand sides of (4)–(6) represent the linear interaction of the perturbation with the horizontal mean state, and we have assumed $\overline{\mathbf{u}} = 0$. The right-hand sides represent the nonlinear interaction of the perturbation with the turbulence field. These nonlinear interactions are complicated and, in general, will both transfer energy to the perturbations and extract energy from them, that is, both force them and damp them.

We propose to model the damping effect of turbulence on the perturbations in terms of an eddy viscosity and diffusivity, and thus write

$$\frac{\partial \mathbf{u}'}{\partial t} + \nabla P' - b'\hat{\mathbf{z}} = \nabla \cdot \{K[\nabla \mathbf{u}' + (\nabla \mathbf{u}')^{\mathrm{T}}]\} + S_u, \tag{7}$$

$$\frac{\partial b'}{\partial t} + w'N^2 = \nabla \cdot (K \nabla b') + S_b. \tag{8}$$

Here the S_u and S_b terms represent the turbulent forcing effect.

Modeling the damping effect as an eddy viscosity and diffusivity is plausible for two reasons. First, the effects of eddies on the mean state of the convective boundary layer, that is, the horizontal mean of the right-hand sides of (1) and (2), can be modeled quite successfully by a combination of a (local) eddy viscosity and diffusivity together with a countergradient contribution (e.g., Holtslag and Boville 1993) or a mass-flux contribution (e.g., Siebesma et al. 2007) to capture nonlocal and upgradient transport. Here, since we are interested in the effects of turbulence on the eddies themselves, that is, the right-hand sides of (4) and (5), rather than the mean state, we retain only the eddy viscosity and diffusivity contribution. Second, for three-dimensional turbulence, an eddy viscosity and diffusivity is considered to be a reasonable model of the effects of subgrid-scale eddies on resolved scales, and is widely used in LES.

For the idealized analysis in section 3, we will take K to be uniform. For the numerical linear stability analysis of section 4, we will assume that a typical K profile of the form and amplitude widely used in modeling the effect of eddies on the mean state of the convective boundary layer is also appropriate to model the turbulent damping of the eddies themselves.

3. Idealized analysis

Some progress can be made analytically by assuming a constant unstable mean stratification $N^2 < 0$ and constant K. We also neglect S_u and S_b for now; we shall return to them in section 4. Dropping the primes for clarity, (7), (8), and (6) then become

$$\frac{\partial \mathbf{u}}{\partial t} + \nabla P - b\hat{\mathbf{z}} = K\nabla^2 \mathbf{u}, \tag{9}$$

$$\frac{\partial b}{\partial t} + wN^2 = K\nabla^2 b, \tag{10}$$

$$\nabla \cdot \mathbf{u} = 0. \tag{11}$$

With these assumptions, (9)–(11) are formally equivalent to the governing equations for Rayleigh–Bénard convection with a Prandtl number of unity, (e.g., Emanuel 1994, chapter 3) and much of the following is implicit in the discussion of that problem. For simplicity we assume an infinite horizontal domain and free-slip boundaries at $z = 0, z_*$.

The symmetries of the constant-coefficient equations, (9)–(11), imply that they have eigenmode solutions proportional to $\exp[i(\mathbf{k} \cdot \mathbf{x} - \omega t)]$ (or the real part of a constant multiple thereof, in order to satisfy the boundary conditions), where $\mathbf{k}$ is the wavevector and ω is the (complex) frequency. It is enough to consider the two-dimensional x–z vertical slice case, since we are free to orient the horizontal axes so that the y component of the velocity and of the wavevector vanish. The linearized equations are then

$$(K|\mathbf{k}|^2 - i\omega)u + ikP = 0, \tag{12}$$

$$(K|\mathbf{k}|^2 - i\omega)w + imP - b = 0, \tag{13}$$

$$(K|\mathbf{k}|^2 - i\omega)b + wN^2 = 0, \tag{14}$$

$$ku + mw = 0, \tag{15}$$

where $(u, w) = \mathbf{u}$ and $(k, m) = \mathbf{k}$. Eliminating u, w, b, and P then leads to

$$\omega = \pm\left(\frac{k^2N^2}{k^2+m^2}\right)^{1/2} + iK(k^2+m^2). \tag{16}$$

Recalling that $N^2 < 0$, this gives a growth rate

$$r = -\mathrm{Im}(\omega) = \pm\left[\frac{k^2(-N^2)}{k^2+m^2}\right]^{1/2} - K(k^2+m^2). \tag{17}$$

Here the first term (with a + sign) represents the tendency for modes to grow due to the unstable stratification. It is small for small k because such modes are inefficient at extracting energy from the unstable stratification, and it saturates at around $|N|$ for $k \gtrsim m$. The second term represents the damping due to viscosity and diffusivity. It increases in magnitude as k and m increase.

Now consider the fastest growing (or slowest decaying) mode. For a given k, the growth rate (17) increases as m decreases. However, the vertical scale of growing modes will be limited by the domain depth, so we set $m = \pi/z_*$. For this m, the value of k that gives the maximum r is determined by setting $\partial r/\partial k = 0$, giving

$$(k^2+m^2)^{3/2} = \frac{m^2|N|}{2kK}. \tag{18}$$

Our hypothesis is that the maximum growth rate is close to zero, in which case (17) implies

$$k|N| \approx K(k^2+m^2)^{3/2}. \tag{19}$$

Substituting from (18) then gives

$$k^2 \approx \frac{1}{2}m^2 \approx \frac{1}{2}\frac{\pi^2}{z_*^2}. \tag{20}$$

Thus, the horizontal scale of the fastest growing mode is comparable to its vertical scale.

Substituting these values of k and m in (19) gives

$$K \approx cz_*^2|N|, \tag{21}$$

where $c = 2/(3^{3/2}\pi^2)$ is a dimensionless constant.[1] Now, the vertical velocity scaling for the convective boundary layer is usually expressed in terms of the surface potential temperature flux Q_* (Deardorff 1970):

$$w_*^3 = gz_*Q_*/\theta_{00}. \tag{22}$$

Writing the potential temperature flux in terms of the eddy diffusivity gives

$$Q_* \approx -K\frac{\partial\theta_0}{\partial z} \approx -KN^2\theta_{00}/g. \tag{23}$$

So, eliminating Q_* between (22) and (23) allows the vertical velocity scale to be expressed in terms of $|N|$:

$$w_*^3 \approx z_*K|N^2|. \tag{24}$$

Finally, eliminating $|N|$ between (21) and (24) gives

$$K \approx c^{2/3}z_*w_*. \tag{25}$$

This scaling of K agrees with that predicted by more conventional convective boundary layer scaling theory (e.g., Holtslag 1998).

For a realistic convective boundary layer N^2 varies strongly with height and (23) will no longer hold locally. Nevertheless (21), (24), and (25) should still be expected to hold for some suitable average values of K and N^2, as sampled by the structure of the marginally stable mode, and would also be expected on dimensional grounds.

4. Numerical linear stability analysis

The above idealized analysis suggests that the marginal stability hypothesis is plausible. However, since there are only a few dimensional parameters in this problem, other plausible arguments could lead to the same predicted scalings. Moreover, in a realistic convective boundary layer the stratification is not uniform; $-\partial\theta_0/\partial z$ peaks strongly near the surface. Therefore, smaller-scale modes confined near the surface will experience a stronger unstable mean stratification than larger-scale modes. There is thus a competition between the preferential growth of small scales due to the instability and the preferential damping of small scales by the eddy viscosity and diffusivity, and it is not obvious a priori which one should dominate. To address these points a more quantitative analysis is carried out for a realistic potential temperature profile.

The potential temperature profile used is shown in Fig. 1. It is taken from an LES of a dry convective boundary layer solving the nonlinear Boussinesq equations and using a Smagorinsky turbulence closure. The case is similar to that of Sullivan and Patton (2011). Starting from an idealized, well-mixed initial potential temperature profile in the convective boundary layer, capped by a strong inversion above 1000 m and with an imposed weak background geostrophic velocity of

[1] In the present notation the Rayleigh number is given by $R_a = |N^2|z_*^4/K^2$, and the constant c is equal to one upon the square root of the critical Rayleigh number for Rayleigh–Bénard convection with free-slip boundaries (Emanuel 1994, section 3.1).

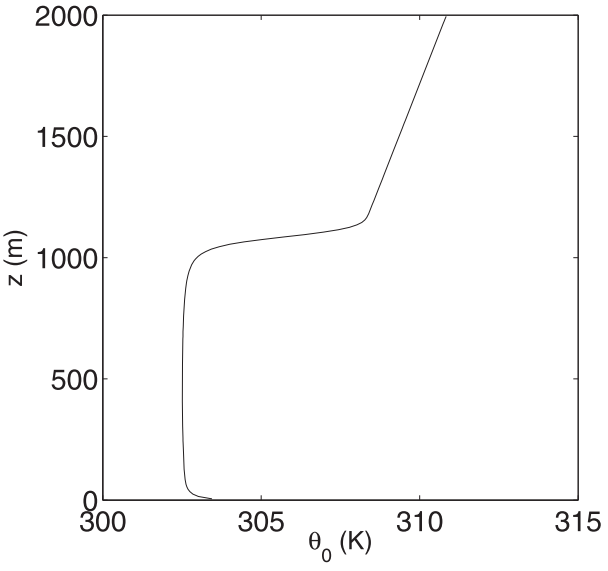

FIG. 1. Background potential temperature profile for the numerical linear stability calculations.

$1\,\mathrm{m\,s^{-1}}$, the boundary layer is forced by a constant surface potential temperature flux $Q_* = 0.24\,\mathrm{K\,m\,s^{-1}}$. The horizontal domain is 9.6 km × 9.6 km with doubly periodic boundary conditions, discretized on a grid with horizontal spacing $\Delta x = 25\,\mathrm{m}$. In the vertical it has a rigid lid at 2000 m with grid spacing $\Delta z = 10\,\mathrm{m}$. The simulation was spun up for 3.5 h, corresponding to about $25t_*$ (see Sullivan and Patton 2011) where $t_* = z_*/w_*$ is the eddy turnover time. The potential temperature profile was then diagnosed as a horizontal mean and a 0.5-h ($\approx 4t_*$) time average. (This averaging time should be sufficient for a first-order quantity such as potential temperature, and increasing the averaging period did not produce any significant differences in the mean potential temperature profile.) For this profile $z_* \approx 1180\,\mathrm{m}$, giving $w_* \approx 2.1\,\mathrm{m\,s^{-1}}$.

To test the marginal stability hypothesis a numerical linear stability analysis was carried out. The Boussinesq equations, (7), (8), and (6), were used, with $\overline{b}$ determined by the potential temperature profile shown in Fig. 1. The disturbances were assumed proportional to $\exp(ikx)$ so that horizontal derivatives could be evaluated exactly. The linear equations were discretized in the vertical on a uniform grid of resolution $\Delta z = 10\,\mathrm{m}$ with a Lorenz grid placement of θ, as in the LES model. Seeking solutions proportional to $\exp(-i\omega t)$ then leads to a vertical one-dimensional eigenvalue problem for ω, which was solved numerically.

The numerical stability analysis was carried out for a range of values of k, corresponding to horizontal scales ranging from a fraction of z_* to several times z_*. For each value of k, the linear mode with the fastest growth rate was found; for the case with zero eddy viscosity and diffusivity, that growth rate is plotted with the circular symbols in Fig. 2. It is seen that the growth rate increases almost linearly with horizontal wavenumber k. Thus, the modes with shortest horizontal scale do indeed grow fastest, consistent with the statement made in the first paragraph of section 1. However, in contrast to the predictions of the idealized analysis (section 3), the growth rate does not asymptotically approach a constant value for $k \gtrsim \pi/z_*$. In the present case with nonuniform stratification, as k increases the fastest growing modes become increasingly confined near the lower boundary (see Fig. 3 below) where they experience more strongly unstable stratification.

The analysis was then repeated with the inclusion of eddy viscosity and diffusivity in the u, w, and θ equations to represent the damping effects of the turbulence. The eddy viscosity and diffusivity were assumed isotropic, with vertical profile given by Holtslag (1998):

$$K = z_* w_* \tilde{k} \left[\left(\frac{u_*}{w_*} \right)^3 + 39 \tilde{k} \hat{z} \right]^{1/3} \hat{z} (1 - \hat{z})^2, \qquad (26)$$

where u_* is the friction velocity, $\tilde{k} = 0.4$ is von Kármán's constant, and $\hat{z} = z/z_*$ is the height normalized by the boundary layer depth. Here the friction velocity is very small, ($u_* \approx 0.08 w_*$; Sullivan and Patton 2011), so it has negligible effect on the results. The full momentum and local angular momentum conserving form of the eddy viscosity term $\nabla \cdot \boldsymbol{\sigma}$ is used, with $\boldsymbol{\sigma} = K[\nabla \mathbf{u} + (\nabla \mathbf{u})^{\mathrm{T}}]$, and with no-slip boundary conditions at the bottom and top boundaries.

In the viscous case, selecting the linear mode with the fastest growth rate (or slowest decay rate) no longer picks out the boundary layer modes of interest because these are generally damped, whereas gravity modes confined to the region above the boundary layer (as well as the Lorenz grid computational mode; Holdaway et al. 2012) have growth rates close to zero. Therefore, instead, for each k, we identify the mode with the largest rate of buoyant production of kinetic energy. In the inviscid case this mode of maximum kinetic energy production is also the fastest growing mode. In the viscous case the mode of maximum kinetic energy production is generally similar in structure to that in the inviscid case (except when kz_* is small) but is neutral or damped.

The triangular symbols in Fig. 2 show the growth rates of the mode of maximum kinetic energy production for each k in the viscous case. All of the modes are now either neutral or damped. There is a maximum growth rate close to zero for modes with $k \approx \pi/z_*$. For these modes, the turbulent damping effect almost completely

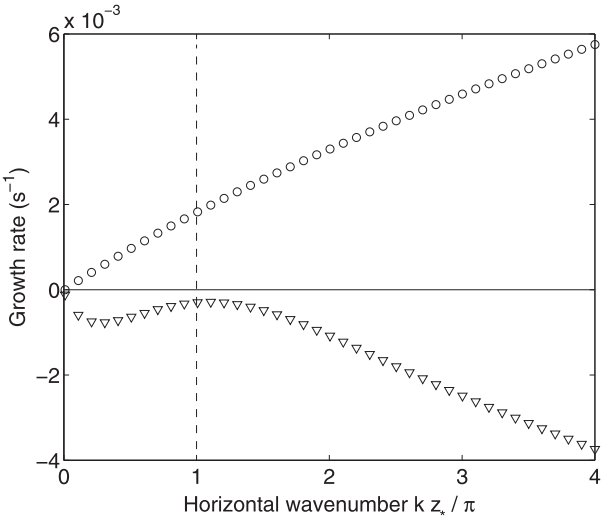

FIG. 2. Growth rate vs normalized horizontal wavenumber ignoring eddy viscosity and diffusivity (circles) and allowing for eddy viscosity and diffusivity (triangles). For each horizontal wavenumber, a linear stability analysis is carried out and the mode that has the strongest buoyant production of kinetic energy is selected. The dashed vertical line indicates a horizontal wavenumber $k = \pi/z_*$, where z_* is the boundary layer depth.

cancels the growth due to the unstable stratification, consistent with the marginal stability hypothesis, despite the simple form of the eddy viscosity and diffusivity used to model the turbulent damping effect.

Modes with $k \approx 0$ also have growth rate close to zero. The idealized analysis, on the other hand, predicts a finite damping rate as $k \rightarrow 0$ with finite m [(17)]. Examination of the mode structures shows that the small-k viscous modes in Fig. 2 are dominated by large amplitude above the boundary layer where K is negligible and have only small amplitude in the boundary layer itself; thus both the unstable stratification near the surface and the viscous damping have only a small effect on these modes.

Modes with large k are strongly damped. For large k the viscous damping effect overwhelms the instability due to stratification, as it does in the idealized analysis. To sustain a turbulent quasi equilibrium, those modes that are damped in the linear analysis must be maintained by turbulent forcing by eddies of other scales—the S_u and S_b terms in (7) and (8).

Figure 3 shows the vertical structure of w for the mode of maximum kinetic energy production for $kz_*/\pi = 1, 2,$ and 3 in the inviscid and viscous cases. The results confirm that as the horizontal scale shrinks the vertical scale also shrinks, so that the mode feels, on average, a more strongly unstable stratification. The viscous modes are slightly deeper and less skewed toward the bottom boundary than their inviscid counterparts. For $kz_*/\pi \approx 1$ the mode of maximum kinetic energy production fills the depth of the boundary layer, especially in the viscous case.

We have repeated this calculation for a number of other potential temperature profiles corresponding to different boundary layer depths and different surface potential temperature fluxes. In all cases similar results were found, consistent with a $k = \pi/z_*$ mode being close to marginal stability. Across these cases the maximum K varied by over 50%, thus providing some confirmation of the scalings predicted by the hypothesis, albeit over a fairly limited parameter range.

5. Summary and discussion

We hypothesize that the dry convective atmospheric boundary layer is marginally stable when the damping effects of turbulence are taken into account, and that the preferential damping of small scales by the turbulence means that the marginally stable mode has horizontal and vertical scale comparable to the boundary layer depth. If these damping effects are modeled by an eddy viscosity and diffusivity, then an idealized analysis predicts that the magnitude of the eddy viscosity follows the well-known scaling $K \sim z_* w_*$, and supports the idea that the marginal mode has length scale $\sim z_*$. A detailed linear stability analysis for a realistic background potential temperature profile also supports the hypothesis.

Note that the hypothesis only predicts the magnitude of the eddy viscosity, not the details of its vertical profile. Further physical assumptions would be needed to predict the profile.

The hypothesis assumes an equilibrium between the growth of boundary layer eddies due to instability and their forcing and damping by turbulence. Such an equilibrium might not hold if there is a rapid change in forcing or if the boundary layer moves over surfaces with different properties. In the absence of viscosity the growth time scale of the $kz_*/\pi = 1$ mode is a little over 500 s, very close to z_*/w_* (Fig. 2). This suggests that the equilibration time scale is also of this order. Such an equilibration time scale is mentioned by Kaimal et al. (1976), Schmidt and Schumann (1989), and is consistent with simple dimensional arguments and also with the initial behavior in numerical turbulent decay experiments (e.g., Nieuwstadt and Brost 1986). The marginal stability hypothesis can be expected to hold on time scales longer than this turbulent equilibration time scale.

In LES results the horizontal wavenumber of the spectral peak in w and in vertical potential temperature flux is observed to decrease with height in the lowest part of the boundary layer below the mixed

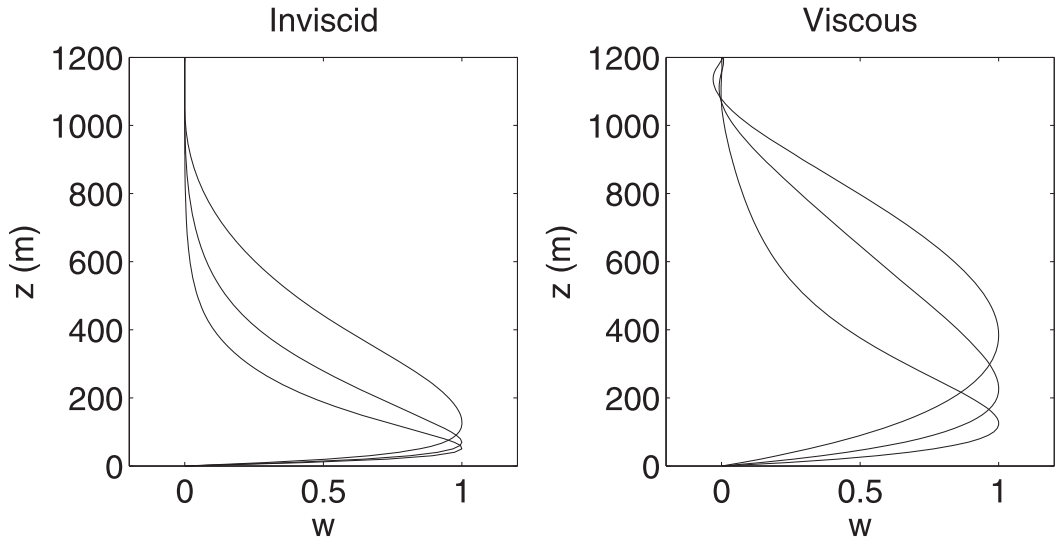

FIG. 3. The w structure of the mode of maximum kinetic energy production for $kz_*/\pi = 1, 2$, and 3. (left) Inviscid case; (right) viscous case. In each case the mode with deepest structure corresponds to $kz_*/\pi = 1$ and the mode with shallowest structure corresponds to $kz_*/\pi = 3$.

layer (e.g., Kaimal et al. 1976). Some authors have interpreted this as indicating that the large thermals in the boundary layer grow through a merging of smaller-scale plumes as they rise from the surface (Mellado et al. 2016). Others, however, argue that small-scale potential temperature perturbations below the mixed layer are quickly dissipated and there is no sign of merger (Schmidt and Schumann 1989). The results shown in Fig. 3 may be relevant to this dependence of the spectral peak on height. Also, the results shown in Fig. 2 support the idea that the largest-scale eddies in the dry convective boundary layer grow primarily by extracting energy from the unstable background potential temperature profile rather than by an upscale energy cascade.

In this note we have focused on the case of very weak background horizontal wind, for which $u_* \approx 0$ and the effects of background shear on the boundary layer turbulence may be neglected. It seems plausible that, even in the presence of a significant background horizontal wind, a nonlinear turbulent equilibrium could be achieved in which instability of the mean flow provides the energy source for the turbulence and turbulent dissipation mechanisms provide the sink. In that case a similar marginal stability hypothesis might hold, though we have not investigated this.

This note highlights a robust dynamical negative feedback controlling the strength and the length scales of the turbulence in the convective boundary layer. One of the main motivations for our interest in this problem is its possible relevance to moist cumulus convection. First, cumulus updrafts for shallow convection have been observed to originate in the boundary layer (LeMone and Pennell 1976), so the length scales of cumulus clouds, at least near cloud base, are expected to be related to the boundary layer eddy length scales. Second, it is possible that similar arguments or extensions of them might be applicable to the turbulent behavior in moist cumulus convection above the boundary layer. For example, there is currently a great deal of uncertainty over turbulent entrainment and detrainment rates for cumulus convection and how to represent them in weather and climate models (de Rooy et al. 2013), and model behavior can be very sensitive to how they are represented (e.g., Romps 2016, and references therein). Any robust constraints on the possible behavior would be very useful.

Acknowledgments. We thank three anonymous reviewers for their constructive comments and for pointing out some relevant literature. This work was funded by the Natural Environment Research Council under the ParaCon program, Grant NE/N013123/1.

REFERENCES

Atkinson, B. W., and J. W. Zhang, 1996: Mesoscale shallow convection in the atmosphere. *Rev. Geophys.*, **34**, 403–431, https://doi.org/10.1029/96RG02623.

Barry, L., G. C. Craig, and J. Thuburn, 2000: A GCM investigation into the nature of baroclinic adjustment. *J. Atmos. Sci.*, **57**, 1141–1155, https://doi.org/10.1175/1520-0469(2000)057<1141:AGIITN>2.0.CO;2.

Betts, A. K., and M. J. Miller, 1986: A new convective adjustment scheme. Part II: Single column tests using GATE wave,

BOMEX, ATEX, and Arctic air-mass data sets. *Quart. J. Roy. Meteor. Soc.*, **112**, 693–710, https://doi.org/10.1002/qj.49711247308.

Ching, J., R. Rotunno, M. LeMone, A. Martilli, B. Kosovic, P. A. Jimenez, and J. Dudhia, 2014: Convectively induced secondary circulations in fine-grid mesoscale numerical weather prediction models. *Mon. Wea. Rev.*, **142**, 3284–3302, https://doi.org/10.1175/MWR-D-13-00318.1.

Deardorff, J. W., 1970: Convective velocity and temperature scales for the unstable planetary boundary layer and Rayleigh convection. *J. Atmos. Sci.*, **27**, 1211–1213, https://doi.org/10.1175/1520-0469(1970)027<1211:CVATSF>2.0.CO;2.

de Rooy, W. C., and Coauthors, 2013: Entrainment and detrainment in cumulus convection: An overview. *Quart. J. Roy. Meteor. Soc.*, **139**, 1–19, https://doi.org/10.1002/qj.1959.

Emanuel, K. A., 1994: *Atmospheric Convection*. Oxford University Press, 580 pp.

——, J. D. Neelin, and C. S. Bretherton, 1994: On large-scale circulations in convecting atmospheres. *Quart. J. Roy. Meteor. Soc.*, **120**, 1111–1143, https://doi.org/10.1002/qj.49712051902.

Garratt, J. R., 1992: *The Atmospheric Boundary Layer*. Cambridge University Press, 316 pp.

Holdaway, D., J. Thuburn, and N. Wood, 2012: Comparison of Lorenz and Charney-Phillips vertical discretisations for dynamics-boundary layer coupling. Part II: Transients. *Quart. J. Roy. Meteor. Soc.*, **139**, 1087–1098, https://doi.org/10.1002/qj.2017.

Holtslag, A. A. M., 1998: Modelling of atmospheric boundary layers. *Clear and Cloudy Boundary Layers*, A. A. M. Holtslag and P. G. Duynkerke, Eds., North Holland Publishers, 85–110.

——, and B. A. Boville, 1993: Local versus nonlocal boundary-layer diffusion in a global climate model. *J. Climate*, **6**, 1825–1842, https://doi.org/10.1175/1520-0442(1993)006<1825:LVNBLD>2.0.CO;2.

Kaimal, J. C., J. C. Wyngaard, D. A. Haugen, O. R. Coté, Y. Izumi, S. J. Caughey, and C. J. Readings, 1976: Turbulence structure in the convective boundary layer. *J. Atmos. Sci.*, **33**, 2152–2169, https://doi.org/10.1175/1520-0469(1976)033<2152:TSITCB>2.0.CO;2.

LeMone, M. A., and W. T. Pennell, 1976: The relationship of trade wind cumulus distribution to subcloud layer fluxes and structure. *Mon. Wea. Rev.*, **104**, 524–539, https://doi.org/10.1175/1520-0493(1976)104<0524:TROTWC>2.0.CO;2.

Lindzen, R. S., and B. Farrell, 1980: The role of polar regions in global climate and a new parameterization of global heat transport. *Mon. Wea. Rev.*, **108**, 2064–2079, https://doi.org/10.1175/1520-0493(1980)108<2064:TROPRI>2.0.CO;2.

Mellado, J. P., C. C. van Heerwaarden, and J. R. Garcia, 2016: Near-surface effects of free atmospheric stratification in free convection. *Bound.-Layer Meteor.*, **159**, 69–95, https://doi.org/10.1007/s10546-015-0105-x.

Nieuwstadt, F. T. M., and R. A. Brost, 1986: The decay of convective turbulence. *J. Atmos. Sci.*, **43**, 532–546, https://doi.org/10.1175/1520-0469(1986)043<0532:TDOCT>2.0.CO;2.

Pandey, A., J. D. Scheel, and J. Schumacher, 2018: Turbulent superstructures in Rayleigh-Bénard convection. *Nat. Commun.*, **9**, 2118, https://doi.org/10.1038/s41467-018-04478-0.

Piotrowski, Z. P., P. K. Smolarkiewicz, S. P. Malinkowski, and A. A. Wyszogodzki, 2009: On numerical realizability of thermal convection. *J. Comput. Phys.*, **228**, 6268–6290, https://doi.org/10.1016/j.jcp.2009.05.023.

Romps, D. M., 2016: The stochastic parcel model: A deterministic parameterization of stochastically entraining convection. *J. Adv. Model. Earth Syst.*, **8**, 319–344, https://doi.org/10.1002/2015MS000537.

Schmidt, H., and U. Schumann, 1989: Coherent structure of the convective boundary layer derived from large-eddy simulations. *J. Fluid Mech.*, **200**, 511–562, https://doi.org/10.1017/S0022112089000753.

Siebesma, A. P., P. M. M. Soares, and J. Teixeira, 2007: A combined eddy-diffusivity mass-flux approach for the convective boundary layer. *J. Atmos. Sci.*, **64**, 1230–1248, https://doi.org/10.1175/JAS3888.1.

Stevens, R. J. A. M., A. Blass, X. Zhu, R. Verzicco, and D. Lohse, 2018: Turbulent thermal superstructures in Rayleigh-Bénard convection. *Phys. Rev. Fluids*, **3**, 041501, https://doi.org/10.1103/PhysRevFluids.3.041501.

Stone, P. H., 1978: Baroclinic adjustment. *J. Atmos. Sci.*, **35**, 561–571, https://doi.org/10.1175/1520-0469(1978)035<0561:BA>2.0.CO;2.

——, and L. Branscombe, 1992: Diabatically forced, nearly inviscid eddy regimes. *J. Atmos. Sci.*, **49**, 355–367, https://doi.org/10.1175/1520-0469(1992)049<0355:DFNIER>2.0.CO;2.

Sullivan, P., and E. G. Patton, 2011: The effect of mesh resolution on convective boundary layer statistics and structures generated by large-eddy simulation. *J. Atmos. Sci.*, **68**, 2395–2415, https://doi.org/10.1175/JAS-D-10-05010.1.

Tennekes, H., and J. L. Lumley, 1972: *A First Course in Turbulence*. MIT Press, 320 pp.

Vallis, G. K., 1988: Numerical studies of eddy transport properties in eddy-resolving and parameterized models. *Quart. J. Roy. Meteor. Soc.*, **114**, 183–204, https://doi.org/10.1002/qj.49711447910.